INCEEUROPE

10th International Conference
on
Wind Turbine Noise
Dublin – 21st to 23rd June 2023

Noise prediction for wind energy turbines based on CAA methods

Christina Appel, Institute of Aerodynamics and Flow Technology, Wind energy, German Aerospace Center (DLR), Lilienthalplatz 7, 38108 Braunschweig, Germany. Christina.Appel@DLR.de

Summary

The here presented work is part of the HGF (Helmholtz Association of German Research Centres) -funded DLR projects ViSion (Validation of Simulation Tools for the Description of Wind Turbines) and LAiSA (**L**astadaptive & **A**eroakusti**s**che **A**nalyse). In both projects we take part at the IEA Wind Task 39 – Quiet Wind Turbine Technology, code benchmark (1). The initial goal is to predict the turbulent boundary layer trailing edge noise (TBL-TEN) and the turbulent inflow noise (TIN) dominating the overall sound radiation for a 2.3 MW NM80 wind turbine. A comparison with other codes within the framework of IEA Wind Task 39 benchmark is shown in Bertagnolio et al. (2).

A process chain, originally developed by Rautmann (3), is used that breaks down the 3D rotor into individual segments, for each of which 2D CAA (computational aeroacoustics) simulations are performed to calculate the TBL-TEN contribution of each slice. Here this tool chain was picked up and supplemented: The rotation of the rotor, the associated amplitude modulation and the variation of the distance to arbitrary evaluation points for the individual rotor blade sections are considered. With the spatial information of each 2D slice related to the chosen observer point and data about the atmospheric turbulence a turbulent inflow noise model is applied. The individual contributions of TBL-TEN and TIN of the blade segments of the entire rotor are finally summarized and averaged over the rotor revolution. In addition to, e.g. the certification position according to IEC-64100-11 standard, arbitrary positions distributed in space can be specified. Third octave spectra can be exported at single observer points varying over the rotor revolution and OASPL values at spatial distributed positions in order to evaluate noise signatures.

1. Introduction

Sound radiated from a wind turbine originates from numerous noise sources. On the one hand there are mechanical sources, like the gear box and the generator. On the other hand, various aero-acoustic sources of sound are responsible for the sound that is perceived at an observer.

Comparing these two dominant types of noise, the aero-acoustic noise outweighs the overall sound emission of a wind turbine (4). The aero-acoustic noise can be split up into airfoil self-noise and turbulence inflow noise. The self-noise sources, in turn, can be split up into a wide

range of sound mechanisms, which are differentiated in the literature (5). These are vortex shedding noise, separation noise, tip vortex noise, and turbulent boundary-layer trailing-edge noise. For multi megawatt turbines, the TBL-TEN turned out to be the prominent contributor to aero-acoustically generated noise (6). Hence, this paper will concentrate on trailing edge noise, but will show up an extension with commonly used semi-empirical turbulence inflow noise models, like it is done in e.g. the software NAFNoise (7) from the National Renewable Energy Laboratory (NREL).

The objective in the project LAiSA is to build a modular, fast prediction tool for the aero-acoustic footprint on the environment of a wind turbine, which can be coupled easily to the blade element method VAST (Versatile Aeromechanic Simulation Tool) developed by the DLR Institute of Simulation and Software Technology and to tools of the DLR Institute of Atmospheric Physics to cover the realistic inflow conditions and noise propagation in complex terrain. The presented method starts with a computational process chain (3) for predicting TBL-TEN by means of modelled stochastically turbulence (8).

To ensure the speed of the procedure, the rotor blades are abstracted as 2D airfoil sections, where a small number, in the order of 8-10, of sections in the outer third of the blade are already sufficient for a convergent solution. The position of the cuts should be chosen with respect to the spanwise change of the blade airfoil geometry. Finally, the result of this step is the directivity of TBL-TEN for each section, which is then the input for the Turbine acoustic prediction (TAP) tool.

In the next step the radiation angle and distance to an observer is calculated over the rotor revolution. The related factors from the precalculated directivity functions for each section are taken and the OASPL and third octave band values are summed up. The contributions of distance correction, 2D/ 3D correction (9) and convective amplification as a result of rotor blade rotation (10) are added. After all, the results are presented as spectra at single observer points or OASPL signatures of observer groups. The output is available time resolved over the rotor revolutions or averaged.

2. Trailing edge noise prediction via a 2D process chain

The 2D process chain for TBL-TEN was originally established by Rautmann (11) to provide an automated acoustic prediction for trailing edge noise on 2D profiles with the aim to obtain acoustically optimized airfoils. Note, the process chain does not contain an optimizer, but it supports the user to identify the acoustic drivers. The process chain operates via bash scripting the input parameters (e.g airfoil geometry, Reynolds number, angle of attack, chord length) and process parameters (e.g. number of iterations, simulated real time and post processing options). Two different mesh generators for RANS and CAA meshing are involved. For simulations the DLR CFD Code TAU and the DLR CAA code PIANO with the stochastic sound source model FRPM (8) (Fast random particle mesh method) are applied. Finally, a collection of python post processing tools is controlled by the process chain, to generate spectra and directivity outputs. The process chain has been also applied to operate an emulation tool set to provide acoustic predictions by means of a data base (12).

2.1 RANS Simulations

In order to generate a TBL-TEN prediction for a turbine, several characteristic profile sections (slice c1 – c16) are extracted from the rotor blade in the area of the outer third (Figure 1). Referred to the IEA Task 39 benchmark this is part of the benchmark description (1). The operating conditions of the present case are listed in Table 1.

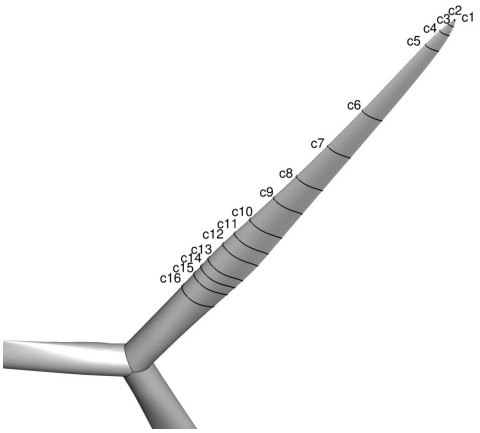

Figure 1 Radial slices

The effective angles of attack and the local incident flow velocities for the blade sections were determined in a first attempt by matching the flow conditions and pressure distribution from a 3D CFD simulation. Later this was done by a much more efficient blade element method (BEM), here the tool Qblade (13). For the flow conditions determined in this way, 2D RANS simulations are performed using the DLR TAU code. A direct use of the 3D RANS calculations is not possible due to the strongly different grid requirements for the use as CAA input. The 2D CFD meshes have been generated with IcemCFD and combine a structured near field and an unstructured farfield, Figure 2. The boundary layer resolution is done carefully with a y+≤1 to yield a sufficient resolution of the viscous sublayer. The structured part contains 118 points normal to the surface and 558 points around the airfoil. In total a CFD mesh contains 520.000 grid points. The applied meshing in done with respect to the best practice suggestions taken from (3). Though the 2D process chain works with parametric inputs, the CFD meshes for each slice are quite similar resolved. For turbulence modelling the Menter SST model (14) has been used. Exemplary the turbulent kinetic energy for the slices c1 -- c8 is shown in Figure 3. All plots in Figure 3 are scaled equally. The RANS simulations are performed using dimensioned quantities, while the CAA calculations are dimensionless. Therefore, the profile length in Figure 3 is already normalized to 1.0 with the respective chord length. One can see the increase of the profile thickness in the inner region. At the same time, the relative values of the TKE decrease due to the lower flow velocities. For section c8, the maximum TKE value is already four times lower than in the outer region.

Air density	*1.231 kg/m2*
Air temperature	*19 °C*
Wind speed	*6.1 m/s*
No wind shear	*-*
Turbulence intensity of the atmosphere	*8.96%*
Turbulence length scale of the atmosphere	*39 m*
Rotor speed	*12.3 rpm*
Pitch angle	*+0.15°*
Yaw angle	*0°*
Transition position suction side	*0.065 chord*
Transition position pressure side	*0.2 chord*

Table 1 Environment conditions

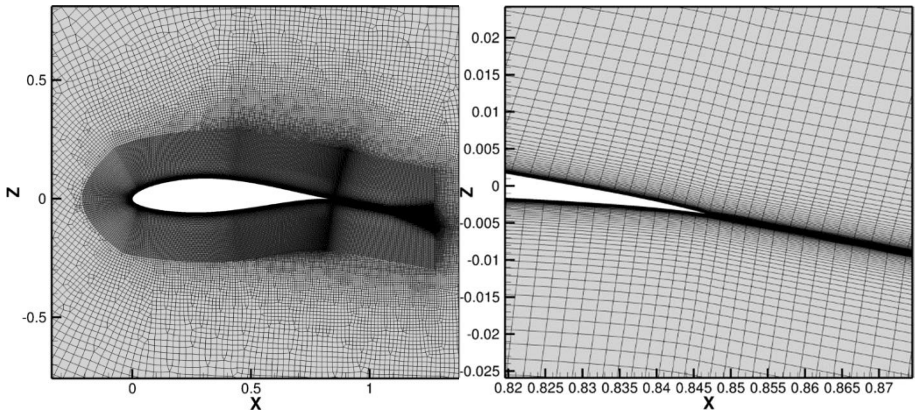

Figure 2 CFD mesh (left) and details near trailing edge (right)

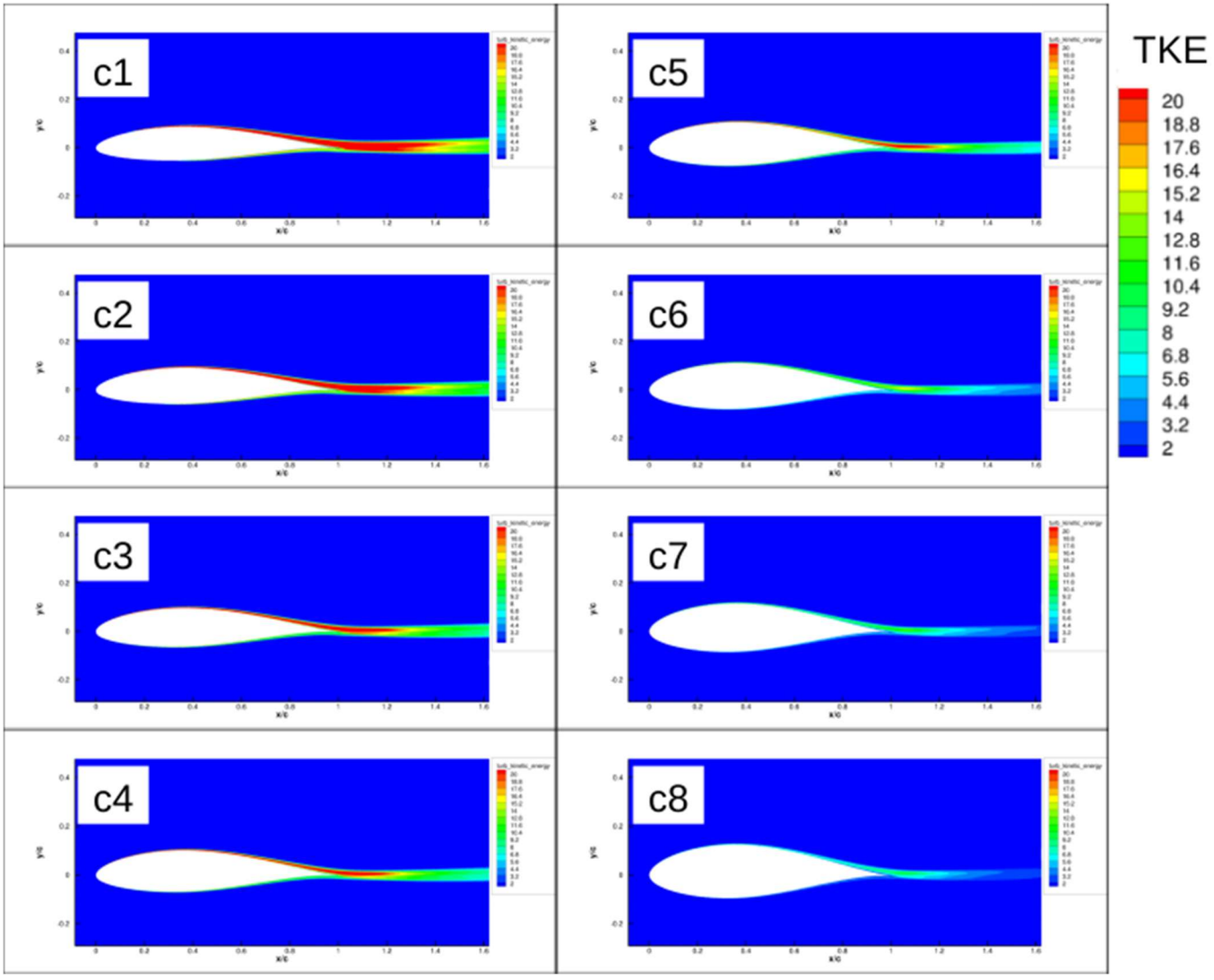

Figure 3 Distribution of turbulent kinetic energy (TKE) in m^2/s^2 for the slices c1 – c8.

2.2 CAA Simulations

The acoustic simulations are based on the APE-4 (acoustic perturbation equation) system with dominating vortex sound source. Acoustical source generation is obtained using the FRPM method (8). For the solution of the perturbation equation system the DLR CAA code PIANO is employed. The spatial discretization is based on the DRP scheme of Tam & Webb (15) and the explicit time integration is done with an alternating LDDRK scheme (16). For the acoustic vortex source, the fluctuating linearized Lamb vector L_i' is modelled. Here the index 0 denotes the

magnitudes of the base flow, the index t those of the turbulence statistics and the prime indicates fluctuating quantities. ϵ_{ijk} is the Levi-Civita symbol.

$$L_i' = -\epsilon_{ijk}\omega_j^0 v_k^t - \epsilon_{ijk}\omega_j^t v_k^0 \quad [1]$$

In the sound propagation calculation with the DLR code PIANO, the sound field is simulated based on the modelled stochastic sound sources. The base flow is also considered in the propagation. For the modelling of the vortex sound sources, the rotation of the fundamental flow is determined from the RANS solution, the turbulent velocities v_k^t are modelled with FRPM and from this the fluctuating vorticity ω_j^t is calculated too. The simulations are evaluated at virtual microphones distributed in a circle with a radius of 2.5 chord lengths around the trailing edge. This allows not only the evaluation of single spectra but also the determination of directivity characteristics. The used CAA grids, generated with the DLR MegaCads grid generator, have been set up parametric, with 1100000 mesh points, and a resolution of 0.0005 chord at the trailing edge and 0.01 chord in the farfield region. This equals a maximal resolved frequency of about 30 kHz in the outer rotor section and 1.7 kHz for the most inner considered blade section.

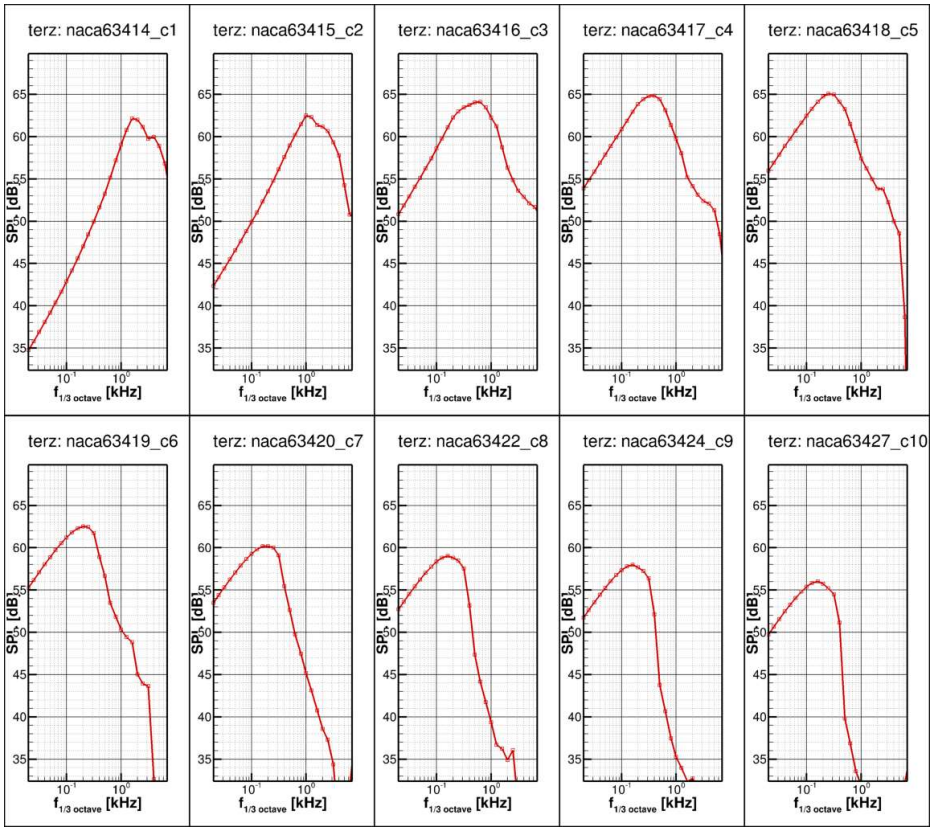

Figure 4 Third-octave spectra of TBL-TEN from 2D CAA calculations. Contributions of each slice, 90° below the trailing edge, perpendicular to the flow vector, normalized to a distance of 1m and a span width of 1m.

In *Figure 4* the third-octave spectra for the slices c1 -- c10, from 2D simulations by means of PIANO/FRPM, are shown. The spectra are normalized to a distance of 1m and a span width of 1m. From the rotor blade tip (c1) to the inner area (c10) one can see that the maximum of the third-octave spectra shifts from about 1.1 kHz to 150 Hz to lower frequencies. The maximum SPL values are between 56 and 65 dB. The highest values are reached at the outer slices c3, c4 and c5. Even further outboard, the flow velocities are higher, but the chord lengths are significantly lower and thus the contribution to trailing edge noise is lower too. Even further inboard the maximum SPL decreases noticeably. These slices will be skipped for the extrapolation of the whole turbine. Additional, flow separations at the inner slices with high

thickness may occur, which have to treated with unsteady RANS calculations and averaging, to ensure proper CAA input data.

3. Summation and Extrapolation – TAP Tool

After the 2D CAA simulations have been carried out for all required sections, the extrapolation for the entire turbine can be performed. In addition to the geometric boundary conditions such as tower height, radial position of the selected 2D sections, number of blades, precone and tilt angle, as well as rotation and wind speed, the directivities from the CAA simulation are read in. Furthermore, observer positions or groups of evaluation points for noise maps are defined.

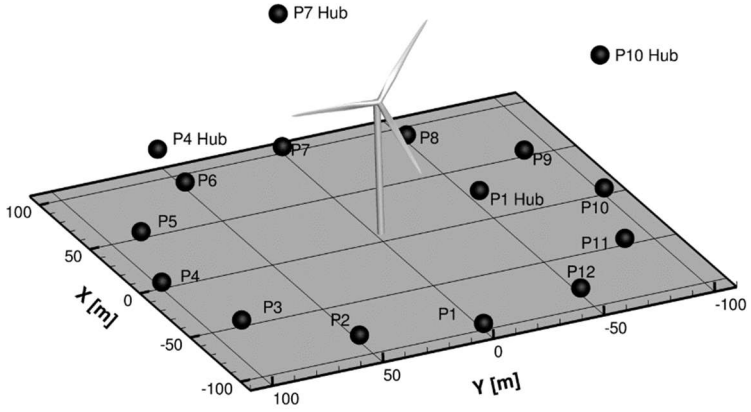

Figure 5 Observer Positions and notation

The observer positions are defined arbitrarily in space in a stationary coordinate system originating in the rotor hub. For the IEA Task 39 benchmark the chosen observers and notation are shown in Figure 5. Further, a rotating coordinate system whose origin is located at the respective trailing edge point of the blade element is defined. The task consists now of carrying out the transformation from one to the other coordinate system and to indicate the observer points with respect to the rotating system. Finally convert it to polar coordinates.
This complex transformation is decomposed into several simple rigid body movements in the form of rotations and displacements. To accomplish this, an affine transformation matrix is used in which all transformations can be mapped with one matrix multiplication each. In detail, the following motion steps are considered:

- Rotation around the tilt angle
- Rotation of the rotor
- Rotation around precone angle
- Rotation around pitch angle
- Shift along radial direction to the position of the slice
- Rotation around twist angle
- Displacement from the threading point (0.75 c) to the trailing edge

This result can be expressed in terms of the polar angles ϕ and θ and the distance r to the observer. Figure 6 from (11) after Ffowcs Williams and Hall (17) illustrates the relationship.

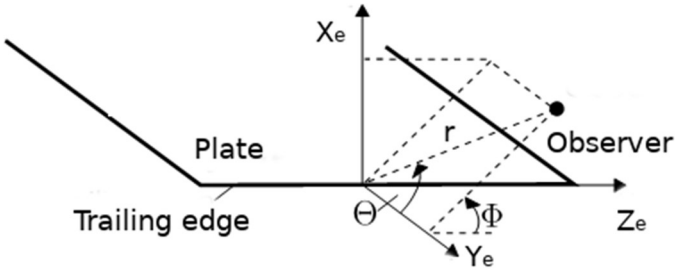

Figure 6 Flow over a semi-infinite plate (11). Polar angles ϕ and $\theta$with respect to an observer.

With this information, the acoustic contribution of the respective segment can be calculated. The beam angle is given by $\theta + \alpha_{eff}$. This allows to choose the related values from the underlying CAA directivity. The reduction due to distance is calculated using $20\,log(r/r_{Mic})$, Eq.[2], where r_{Mic} is the radius of the microphone circle in the CAA simulation and r is the distance trailing edge to observer point. The CAA directivity is 2D but the blade segment should be 3D. This is corrected accordingly to (17): the sound intensity of a semi-infinite plate scales with $sin(\phi)$, Eq.[3]. Furthermore, a 2D/3D correction, Eq.[4] of the far-field sound pressure levels is performed for the individual blade elements, considering the span of the blade segments. This is explained in more detail in Ewert et al. (9). The constant C in Eq.[4] is set to 1.4 according to Fassmann et al.(12). The chord length is c. The influence of the segment width is considered with Eq.[5], the reference width $b_{ref} = 1.0$m.

$$L_{p,distance} = 20\,log\left(\frac{r_{mic}}{r}\right) \quad [2]$$

$$L_{p,si} \quad = 10\,log(sin\,\phi) \quad [3]$$

$$L_{p,2D/3D} = 10\,log\left(\frac{C}{2\pi}\cdot\frac{c}{r_{mic}}Ma_{piano}\right) \quad [4]$$

$$L_{p,width} = 10\,log\left(\frac{b}{b_{ref}}\right) \quad [5]$$

The convective amplification due to rotor motion is considered as a scaling of the directivity D according to Brooks and Burley (10). Here ξ is the angle between the vector of blade leading edge flow and the line connecting the trailing edge to the observer. Ma_{piano} is the Mach number of the flow at slice position.

$$D \propto \frac{2\,sin(\theta/2)^2\,sin\,\phi^2}{\left(1-Ma_{piano}\,cos(\xi)\right)^4} \quad [6]$$

The numerator in the Eq.[6] describes the directivity of high-frequency trailing edge noise. It was analytically derived for trailing edge noise from a semi-infinite flat plate (5) but was also found to be valid for finite airfoils (18) assumed that the angle θ is not too close to 180° and the acoustic wavelength is smaller than the airfoil chord. For low frequency noise, where the acoustic wavelength is much larger than the airfoil chord, the $sin\,\theta/2^2$ term changes into $sin\,\theta^2$. As suggested in (19) respective (10) an exponent of 4.0 is used for the power law.

$$L_{p,Amp} = 40\,log\left(\frac{2\,sin(\theta/2)^2\,sin\,\phi^2}{(1-Ma_{tot}\,cos(\xi))^4}\right) \quad [7]$$

Finally, all terms of L_p can be added, while $L_{p,piano}$ equals to the value from the computed directivities from PIANO.

$$L_p = L_{p,piano} + L_{p,width} + L_{p,distance} + L_{p,2D/3D} + L_{p,sin\,\phi} + L_{p,Amp} \quad [8]$$

This has to be done for all blades and all blade sections. The results can now be presented as OASPL values or 1/3 octave spectra at single or observer positions or grouped positions to

yield a noise map. In *Figure 7* this is done for a 200m times 200m horizontal map on the ground and for a vertical map in a downwind distance of 100m. The OASPL values are averaged over the rotor revolution.

According to the observer positions depicted in *Figure 5* the resulting TBL-TEN spectra are given in *Figure 8*. Each plot shows a set of curves corresponding to the azimuth angle of the rotor. Note there is a small variance with the azimuth angle for positions directly downwind the wind turbine (P1, P7), no variance for downwind hub position (P1hub, P7hub), and a large variance for the most lateral positions (P4, P10, P4 hub, P10 hub).

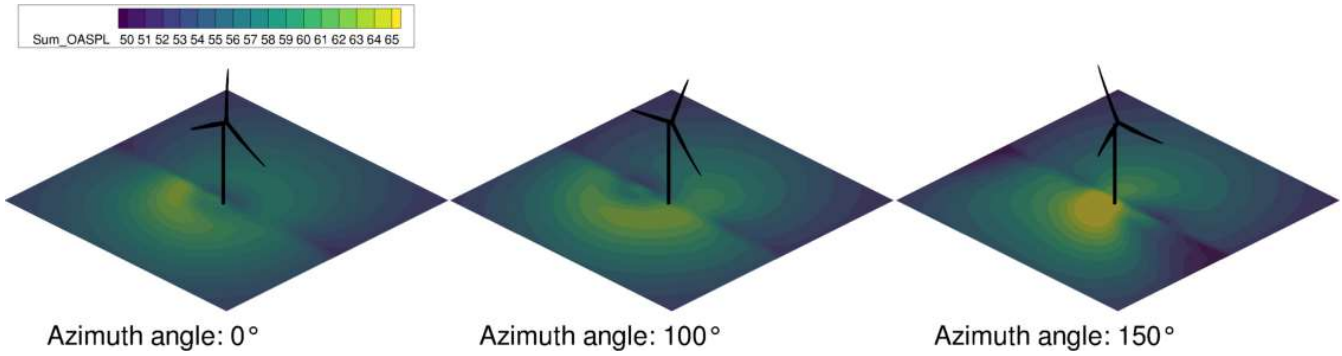

Figure 7 OASPL noise map for the Task 39 benchmark case at different azimuth angles.

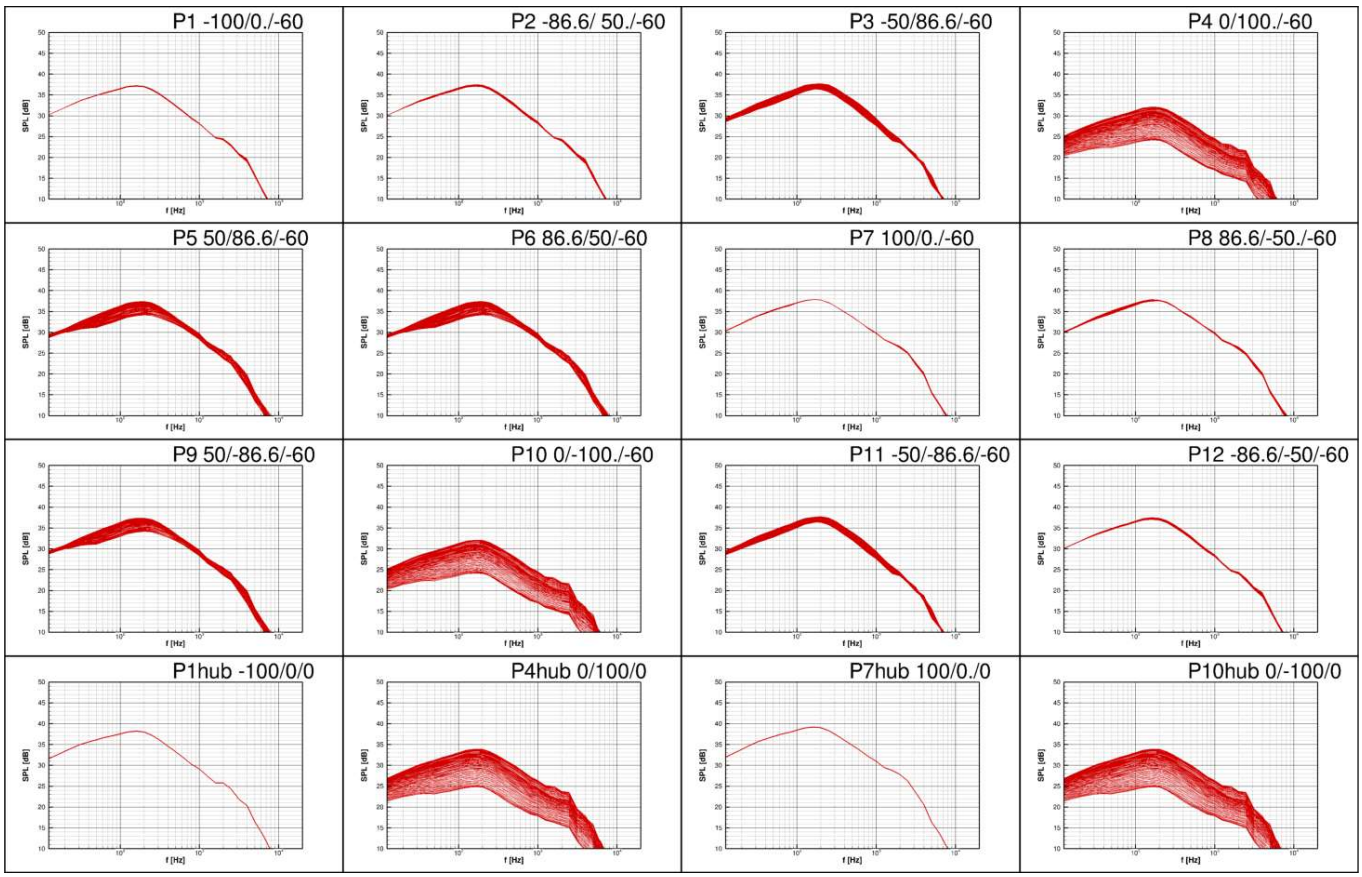

Figure 8 TBL-TEN spectra for benchmark observer positions.

4. Turbulent inflow noise via semi-empiric modelling

There are several methods to model turbulent inflow noise. On the one hand, there are CAA applications, which, however, require a high numerical effort. The high effort, e.g. for the very efficient CFD/CAA method used here, already becomes clear during the generation of the base flow including atmospheric turbulence. Not only the complete wind turbine including the inflow

has to be recorded transiently, but also the near-wall regions on the rotor blades have to be resolved carefully, so that reasonable CAA results can be expected. In addition, the rotor circulation has also to be considered. The actual task of CAA simulation starts only after that. Following from that, for fast predictions on complete wind turbines, only TIN modelling can be considered.

One the other hand there is the analytical model by Amiet and Patterson (20) for TIN. Here the different characteristics of high and low frequency part of the TIN are considered and a smooth transition between both parts is achieved by applying a low frequency correction to the high frequency part. Furthermore, a bunch of simplified semi-empirical models based on the complex model of Amiet and Patterson can be found in literature (21) (22) (23)(25). These models employ basically an equation to model the third octave spectra for the high frequency part (index h) dependent on the wavenumber based on the chord length, as necessary normalized with the wavenumber of energy containing eddies from the inflow, and a low frequency correction (LFC, index L). Due to good results compared with the complex Amiet model, low computational effort and easy implementation, among others the semi-empirical models of Lowson(24) and Moriarty et. al.(25) have been chosen to be implemented in the TAP tool to provide the TIN contribution. In detail the following model equations are applied:

$$SPL_{1/3}^{L} = SPL_{1/3}^{H} + 10\log_{10}(LFC) \quad [9]$$

For the Lowson model:

$$SPL_{1/3}^{H} = 10\,log_{10}\left[\frac{\rho_0^2 c_0^2 \Lambda d}{2r^2} Ma^3 u'^2 K_1^3 (1+K_1^2)^{-7/3}\right] + 58.4 \quad [10]$$

with Λ the turbulent length scale of the atmosphere, $\rho_0$the density, c_0 the speed of sound, d the span, I the turbulence Intensity at the blade, based on the local flow velocity, u'^{2} the mean square turbulence level, $D_L$the low frequency directivity and K_1 the wave number with chord length and the local flow velocity U at the blade.

$$K_1 = \frac{\pi f c}{U} \quad [11]$$

The low frequency correction is defined as:

$$LFC = 10S^2 Ma K_1^2 \beta^{-2} \quad [12]$$

with

$$S^2 = \left(\frac{2\pi K_2}{\beta^2} + \left(1 + 2.4\frac{K_1}{\beta^2}\right)^{-1}\right)^{-1} \quad [13]$$

$$\beta^2 = 1 - Ma^2 \quad [14]$$

Several differences are present in the implemented model of Moriarty:

$$SPL_{1/3}^{H} = 10\log_{10}\left[\frac{\rho_0^2 c_0^4 \Lambda d}{2r^2} Ma^5 K_2^3 I^2 (1+K_2^2)^{-7/3} D_L\right] + 78.4 \quad [15]$$

Here the LFC contains a term to take the effective angle of attack into account:

$$LFC = 10S^2 Ma\left(1 + 9\alpha_{eff}^2\right) Ma K_2^2 \beta^2 \quad [16]$$

$$S^2 = \left(\frac{2\pi K_3}{\beta^2} + \left(1 + 2.4\frac{K_2}{\beta^2}\right)^{-1}\right)^{-1} \quad [17]$$

And two different wavenumbers considering the span and the turbulent length scale are employed:

$$K_2 = \frac{8\pi f \Lambda}{3U} \quad [18]$$

$$K_3 = \frac{\pi f b}{U} \quad [19]$$

In both models finally the $SPL_{1/3}$ is given by:

$$SPL_{1/3} = SPL_{1/3}^{H} + 10\log_{10}\left(\frac{LFC}{(1+LFC)}\right) \quad [20]$$

The low frequency directivity function is in both models the same:

$$D_L = \frac{\sin\theta^2 \sin\phi^2}{(1+Ma\cos\theta)^4} \quad [21]$$

To give an impression of the shape, D_L is plotted in Figure 9 in polar coordinates. With the information about the angles θ and ϕ according to a certain observer position, the value of D_L can be examined at every radial and azimuthal position of the blades.

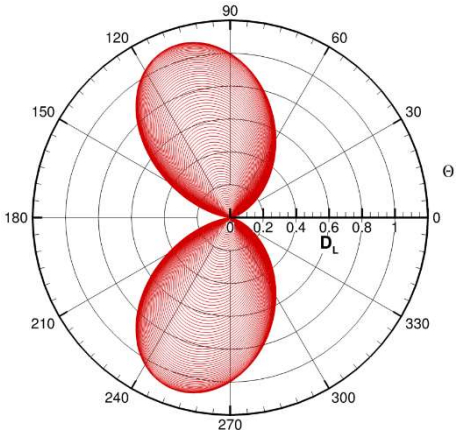

Figure 9 Exemplary directivity function for TIN

The turbulent length scale Λ is direct proportional to the SPL value for TIN, but is not trivial measure on site and shows a broad value range. The model by Moriarty assumes this value as the 2.45 times the hub height, up to a maximum of 73.5m. For the model of Lowson the length scale is set to a free parameter to be chosen by atmosphere or experimental data. Especially in wind tunnel validation experiments, the length scale can be defined exactly by e.g. the size of wind tunnel flow straightener meshes.

Wetz et al. (26) show up the complexity of atmospheric boundary layer measurements and the estimation of parameters like Λ or turbulence intensity. Within the observation period the length scale varies between 29 and 329m, which equals terms of decibels following Eq.[15] a range of more than 10dB. In Figure 10 the resulting TIN spectra for the Lowson and Moriarty model are shown. The turbulence length scale varies between 39m (value from IEA Task 39 Benchmark) and 100m (parameter from (23)).

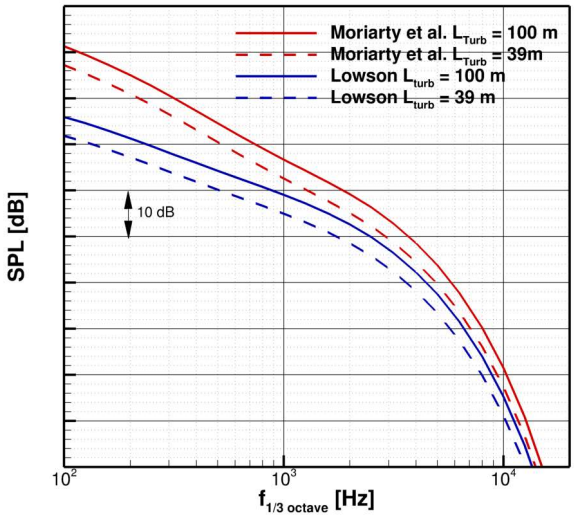

Figure 10 Dependency of turbulence length scale on TIN spectra for models by Lowson and Moriarty

5. Combination of TBL-TEN and TIN sources

The last step is the superposition of both sources. Since both parts are resolved over the rotor revolution, the final result can also be displayed accordingly or output in averaged form. The resulting 1/3 octave spectra are shown in Figure 11. Here the TIN model by Lowson is applied. The red curve set is again the TBL-TEN, the green curves are the TIN spectra. As the levels are much higher than the TEN noise, the superposition curves in black hide the green lines nearly completely.

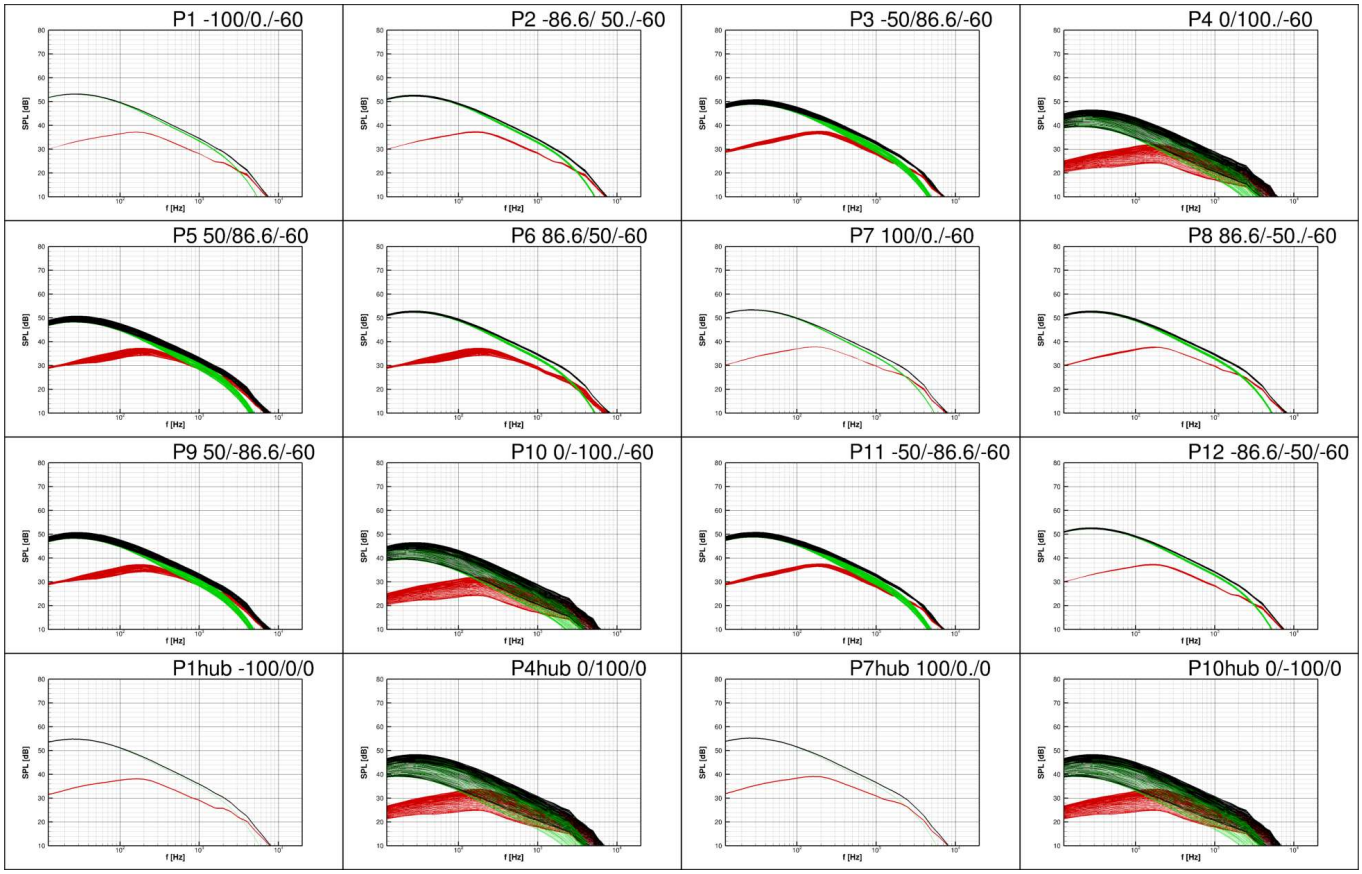

Figure 11 Superposition (black) of TBL-TEN (red) and TIN (green) spectra. TIN model by Lowson.

The TIN dominates the superposed spectra up to a frequency of 300Hz. Due to the impact of the turbulence length scale and the complexity to measure these data from experiments it is difficult to assess the results. On the other hand, there are experimental data sets published by Moriarty et al. and Buck et al. (21) (27), which shows similar behaviour.

6. Conclusions and Outlook

In the current work a high-fidelity CAA method for TBL-TEN noise is combined with extrapolation tool and semi-empirical models for TIN. The efficiency of the CAA method could be kept high and the numerical effort low by using 2D slices of a rotor blade. A complete run for one operational point of a wind turbine takes about 8h on 64 cpus, but could be also done on a desktop machine spending some more time. The extrapolation for several 100 observer points takes only a couple minutes.

Next action items are the implementation of OASPL output for TIN part, to add this to the noise maps too. Furthermore, additional semi-empirical and improved TIN models should be implemented, taking the real atmospheric conditions into account. Moreover, a separation noise model module is planned to be implemented. Also, the option to have more than one wind turbine at the same run in the extrapolation tool TAP is interesting to cover the acoustic

superposition with the rotor azimuth for a group of turbines. Last but not least the validation with experimental field data is an important issue, hence we are looking forward to the first acoustic measurements from the DLR research wind farm WiValdi at Krummendeich.

References

(1) Bertagnolio, F., Madsen, H., Hornung, C., Schepers, G.: IEA Wind Task 39 – Quiet Wind Turbine Technology, Wind Turbine Noise Code Benchmark (Phase I), 2019.
(2) Bertagnolio, F., Fischer, A., Appel, C., Herr, M., Seel, F., Lutz, T., Boorsma, K., Schepers, G., Restrepo Botero, M., Casalino, D., Sucameli, C., Bortolotti, P., Wind turbine noise code benchmark: A comparison and verification exercise. 10th International Conference on Wind Turbine Noise, Dublin – 21st to 23th June 2023
(3) Rautmann, C., Dierke, J., Ewert, R., Hu, N.: Generic Airfoil Trailing-Edge Noise Prediction using Stochastic Sound Sources from Synthetic Turbulence, AIAA 2014-3298
(4) Wagner, S., Bareiss, R., Guidati, G.: Wind turbine noise, Vol. 16823 of Research and Development, Springer, Berlin, 1996.
(5) Brooks, T. F., Pope, D. S., Marcolini, M. A., “Airfoil Self-Noise and Prediction,” Hampton and VA. Langley Research Center,1989.
(6) Oerlemans, S., Fisher, M., Maeder, T., Kögler, K., “Reduction of Wind Turbine Noise Using Optimized Airfoils and Trailing-Edge Serrations,” AIAA Journal, Vol. 47, No. 6, 2009, pp. 1470–1481.
(7) Moriarty, P., NAFNoise User’s Guide, Documentation, https://nwtc.nrel.gov/system/files/nafnoise.pdf, 2005.
(8) Ewert, R.: RPM - the fast Random Particle-Mesh method to realize unsteady turbulent sound sources and velocity fields for CAA applications, AIAA 2007-3506.
(9) Ewert, R., Appel, C., Dierke, J., Herr, M. RANS/CAA Based Prediction of NACA 0012 Broadband Trailing Edge Noise and Experimental Validation, AIAA 2009-3269.
(10) Brooks, T. F., Burley, C. L.: Rotor Broadband Noise Prediction with Comparison to Model Data, AIAA 2001-2210.
(11) Rautmann, C.: Numerical Simulation Concept for Low-Noise Wind Turbine Rotors, DLR Forschungsbericht 2017-35.
(12) Faßmann, B., Reiche, N., Ewert, R., Herr, M., Delfs, J.: Evaluation of Wind Turbine Noise based on Numerical Simulation Methods, AIAA 2018-3924.
(13) Marten, D.: QBlade Guidelines v 0.6, (2012), TU Berlin
(14) Menter, F. R.: Two-equation eddy-viscosity turbulence models for engineering AIAA Journal, Vol. 32, No. 8, August 1994.
(15) Tam, C., Webb, J.: Dispersion-relation-preserving finite difference schemes for computational acoustics. J Comp Phys 107, 262–281, 1993.
(16) Hu, F. Q., Hussaini, M. Y., Manthey, J. L.: Low-dissipation and low-dispersion Runge–Kutta schemes for computational acoustics. J Comp Phys 124, 177–191, 1996.
(17) Ffowcs Williams, J. E., Hall, L.H.: Aerodynmaic sound generation by turbulent flow in the vicinity of a scattering plane. JFM, 40, No. 4, 1970. J Comp Phys 1996;124:177–91.applications, AIAA Journal, Vol. 32, No. 8 1994.
(18) Hutcheson, F.V., Brooks, T.F.: Effects of angle of attack and velocity on trailing edge noise, AIAA 2004-1031, 2004.
(19) Oerlemans, S., Sijtsma, P., Mendez Lopez, B.: Location and quantification of noise sources on a wind turbine, JSV 299 (2007) 869–883.
(20) Paterson, R. W., Amiet, R. K., Noise and Surface Pressure Response of an Airfoil to incident Turbulence, Journal of Aircraft, vol. 8, no. 14, 1977.
(21) Moriarty, P., Migliore, P., Semi-Empirical Aeroacoustics Noise Prediction Code for Wind Turbines, 2003.
(22) Buck, S., Oerlemans, S., Palo, S., Experimental Validation of a Wind Turbine Turbulent Inflow Noise Prediction Code," AIAA Journal, pp. 1495-1506, 2018.

(23) Lowson, M., Assessment and Prediction Of Wind Turbine Noise, Flow Solutions Report, vol. 92, no. 19, 1992.
(24) Lowson, M., Theory and experiment for wind turbine noise. AIAA 94-0119, 1994.
(25) Moriarty, P., Guidati, G., Migliore, P., Recent Improvement of a Semi-Empirical Aeroacoustic Prediction Code for Wind Turbines, AIAA 2004-3041, 2004
(26) Wetz, T., Zink, J., Bange, J., Wildmann, N., Analyses of Spatial Correlation and Coherence in ABL flow with a fleet of UAS, https://doi.org/10.21203/rs.3.rs-2033943/v1
(27) Buck, S., Oerlemans, S., Palo, S., Experimental validation of a wind turbine turbulent inflow noise prediction code. AIAA Journal, Vol. 56, No. 4, April 2018